Application of a non local fatigue stress gradient- weigth function approach to predict the crack nucleation risk induced by Fretting Fatigue

Siegfried Fouvry*, Bruno Berthel

LTDS, Ecole Centrale Lyon, 69134 Ecully, France
* Corresponding author: siegfried.fouvry@ec-lyon.fr

Abstract

Fretting-Fatigue problems are very complex to address due to the multiaxiality and the very sharp stress gradients imposed below the interfaces. Hence, multiaxail and non local fatigue approach must be considered. An experimental cylinder/plane fretting fatigue and plain fretting analysis a 35 Ni Cr Mo 16 low alloyed steel at 10^6 cycles has been performed to investigate the incipient crack nucleation response for various stress gradient conditions. Imposing elastic stress conditions, the Crossland's approach is applied to predict the crack nucleation risk. This analysis confirms that a local stress analysis at the "hot spot" stress located at surface trailing contact border is not suitable. The non local "critical distance" approach which considers the stress loading path at a fixed distance from the "hot spot" improves the prediction but still induce a large discrepancy. Finally, the best predictions are achieved using an alternative non local "weight function" approach where the crack nucleation risk computed at the "hot spot" is weighted by a function expressed as as a linear decreasing expression of the hydrostatic stress gradient operating around the "hot spot" location. The stability of this approach regarding the contact stress field resolution and related application for FEM application is discussed.

Keywords Fretting Fatigue crack nucleation, Stress gradient, Non local fatigue approach, Crossland

1. Introduction

Fretting is a small amplitude oscillatory movement, which may occur between contacting surfaces that are subjected to vibration or cyclic stress. Combined with cyclic bulk fatigue loading, the so-called fretting-fatigue loading can induce catastrophic cracking phenomena which critically reduce the endurance of assemblies [1]. Fretting Fatigue loading can be characterized by the superposition of a heterogeneous cyclic stress gradient related to the contact loading, and a quasi-homogeneous fatigue bulk loading (Fig. 1). The crack nucleation phenomenon is commonly addressed by transposing conventional multi-axial fatigue criteria [2] taking into account or not the stress gradient effects [3, 4]. Indeed, as illustrated in Figure 2, the fretting stressing conditions are characterized by very severe stress gradients which could be one order of magnitude higher than common notch fatigue stress configurations. Non local fatigue approaches are therefore required to predict the cracking risk. Stress averaging approaches [3, 5], or equivalent critical distance methods [4] which consist to consider the stress state at a "critical distance" from the stress "hot spot" are commonly applied to capture the stress gradient effect. However, these approaches, which consider a fixed length scale value are limited when large stress gradient fluctuations are operating. To palliate such limitation, an alternative strategy which consists to weight the prediction given at the "hot spot" location using a linear decreasing function expressed as a function of the gradient of the hydrostatic stress around the hot spot stress location is considered. Introduced by Papadopoulos [6], this approach was simplified by Amargier et al. to predict plain fretting crack nucleation conditions

[7]. The purpose of this research work is to extend this approach for partial slip fretting fatigue situations. This analysis also addresses the influence of the size domain over which the hydrostatic stress gradient is computed thus to establish the stability of this approach regarding the spatial contact stress resolution.

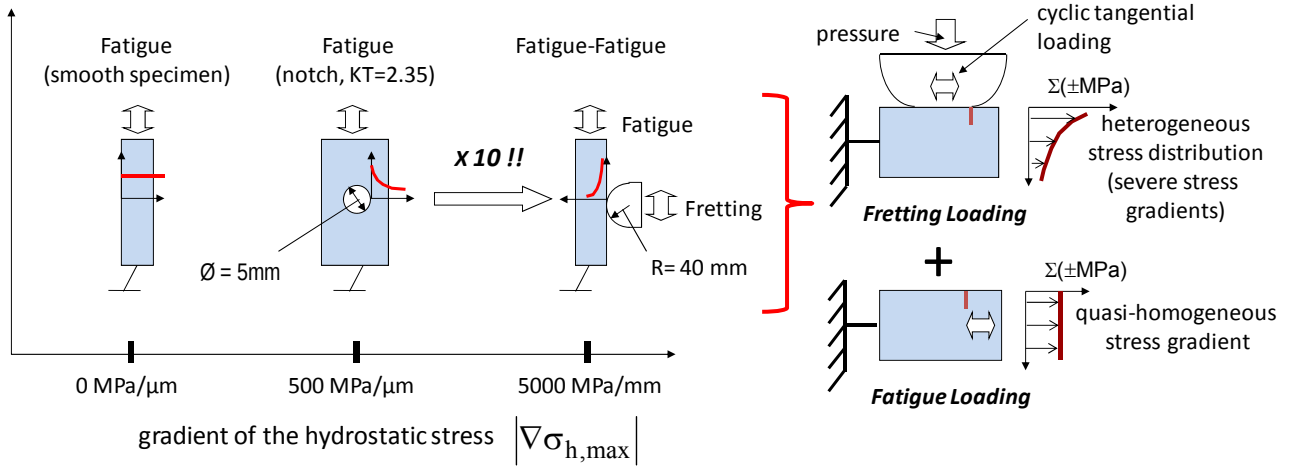

Figure 1. Illustration of the stress condition characterizing the fretting fatigue loading.

2. Materials and experimental procedure

2.1. Materials

The studied material is a tempered a 35 Ni Cr Mo 16 low alloyed steel displaying a tempered Martensitic structure. The original austenite grain size is about Ø =20 µm. The mechanical and fatigue properties of this steel, are summarized in the following table 1.

Table 1. Mechanical and fatigue properties of the studied 35 Ni Cr Mo 16 low alloyed steel.

E(MPa)	ν	$\sigma_{y0.2\%}$ (MPa)	σ_u (MPa)	σ_d (MPa)	τ_d (MPa)	ΔK_{th} (MPa$\sqrt{m}$)
205000	0.3	950	1130	575	386	3.2

E: Young's modulus; ν: Young's modulus, $\sigma_{y0.2\%}$: Yield stress (0.2%); σ_u: ultimate stress; σ_d : traction – compression fatigue limit ($R\sigma = \sigma min/\sigma max = -1$ for 10^7 cycles); τ_d : shear fatigue limite ($R\tau = -1$ for 10^7 cycles); ΔK_{th} : long crack threshold (R=-1).

Chromium 52100 steel was chosen for the cylindrical pads in order to maintain elastically similar conditions whilst simultaneously ensuring that cracks arose only in plane and fatigue 35NiCrMo16 specimens. Both plane and cylindrical pad surfaces were polished to achieved a small Ra=0.05 µm surface roughness.

2.2. Test conditions

As illustrated in Figure 3, two different test apparatuses were involved to quantify respectively the fretting and the fatigue influences in cracking processes.

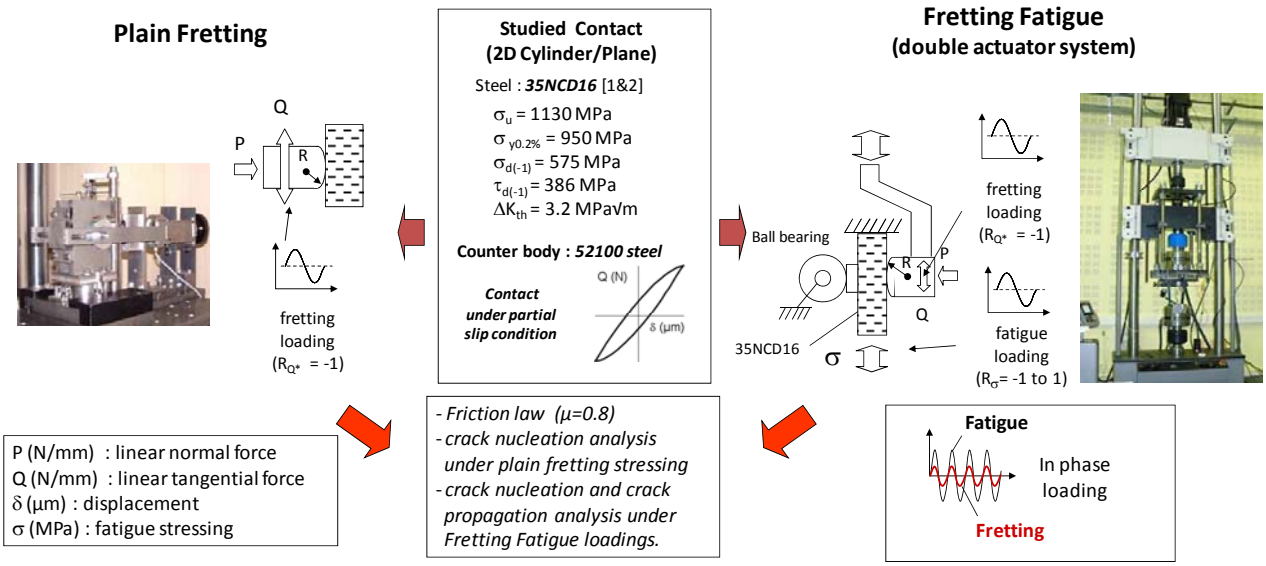

Figure 2. Illustration the experimental strategy based a combined plain fretting and fretting fatigue analysis involving similar contact configurations.

Plain Fretting tests were applied by imposing a nominally static normal force P, followed by a purely alternating cyclic displacement amplitude (δ*), so that an alternating cyclic tangential load Q was generated on the contact surface. During a test, P, Q and δ are recorded, from which the δ - Q fretting loop can be plotted. The studied plane specimen is not subjected to any fatigue stressing.
The fretting fatigue experiments were performed using a dual actuator device inspired by Fellows et al. [8]. This test system allows the separate application and control of fretting and fatigue loadings. Like for the plain fretting, the system is instrumented to measure the contact loading (P, Q*, δ*) but also the fatigue stressing (σ, $R_\sigma=\sigma_{min}/\sigma_{max}$).
In order to analysis both contact pressure, fatigue stress and stress gradient effects, various cylinder radius from R= 20 to 80 mm, Hertzian contact pressures from p_{max}=600 to 1000 MPa and fatigue stress conditions from σ_{max}= 0 and 400 MPa considering two stress ratio Rσ=0.1 and 1.0 were investigated. The details of the studied conditions are compiled in table 2. Note that the lateral width of the cylinder pads (W) was chosen to satisfy plain strain conditions.

3. Experimental results

3.1. Friction analysis

Because the partial contact stress field depends on the coefficient of friction, it is important to establish this value. H. Proudhon et al. show in [10] that the friction coefficient measured at the transition between partial and gross slip conditions (μ_t) may be used to provide a representative value of the friction under partial slip conditions (i.e. $\mu_{PS}=\mu_t$). Figure 3b compares the obtained μ_t

values as a function of the Hertzian contact radius for different contact pressures. A quasi constant evolution is observed which allows us to consider a constant friction value (i.e. $\mu=\mu_{PS}=\mu_t=0.8$).

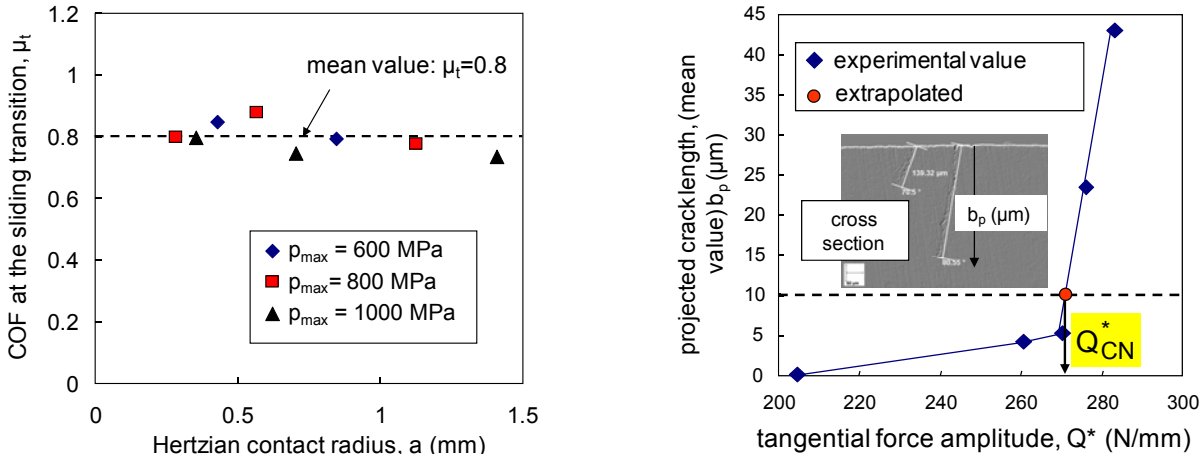

(a) (b)

Figure 3. a) Evolution of the coefficient of friction (COF) at the sliding transition as a function of the contact radius and the maximum Hertzian pressure for the studied interfaces - b) Illustration of the destructive methodology used to identify the crack nucleation condition for plain fretting and fretting fatigue conditions.

Table 2. Compilation of the studied test conditions (PF : plain fretting, FF: fretting fatigue)

	R (mm)	W (mm)	P (N/mm)	σ_{max} (MPa)	Rσ	p_{max} (MPa)	a (mm)	μ_t	Q^*_{CN} (N/mm)	$k=\frac{c}{a}$	e (mm)	$\frac{\sigma_{VM}}{\sigma_Y}$
PF_1	20	3	353	0	0	800	0.28	0.8	186	0.58	-	0.97
PF_2	20	3	552	0	0	1000	0.35	0.8	218	0.71	-	1.05
PF_3	40	5	398	0	0	600	0.42	0.85	271	0.38	-	0.83
PF_4	40	5	707	0	0	800	0.56	0.88	287	0.70	-	0.85
PF_5	40	5	1100	0	0	1000	0.70	0.75	310	0.80	-	0.89
PF_6	80	8	795	0	0	600	0.84	0.79	305	0.72	-	0.62
PF_7	80	8	1414	0	0	800	1.12	0.78	399	0.80	-	0.71
PF_8	80	8	2209	0	0	1000	1.40	0.74	470	0.85	-	0.77
FF_1	80	8	795	100	0.1	600	0.84	-	273	0.75	0.02	0.69
FF_2	80	8	795	200	0.1	600	0.84	-	261	0.76	0.04	0.78
FF_3	80	8	795	400	0.1	600	0.84	-	137	0.88	0.08	0.87
FF_4	40	8	398	100	0.1	600	0.42	-	210	0.58	0.01	0.83
FF_5	40	8	398	200	0.1	600	0.42	-	192	0.62	0.02	0.90
FF_6	40	8	398	400	0.1	600	0.42	-	100	0.83	0.04	0.93
FF_7	80	8	795	200	1	600	0.84	-	300	0.72	-	0.80
FF_8	80	8	795	400	1	600	0.84	-	280	0.74	-	0.97

3.2. Crack nucleation analysis

The cracking investigation consists in identifying the partial fretting loading (i.e. $Q^*<\mu P$) inducing

a threshold crack length after 10^6 cycles. The following methodology is applied: After each fretting test, the plane specimen is cut along the median axis of the fretting scar. Cross section observations are performed to determine the projected crack length (b_p) along the normal of the surface. The polishing process is then repeated twice so that the crack measurement is performed on 6 different planes located along the median axis of the fretting scar. From these six measurements, the maximum projected crack length (b_{pmax}) is determined. This crack analysis is generalized to various tangential force amplitudes in order to plot the evolution of b_{pmax} versus the applied tangential force amplitude (Fig. 3b). Finally, the threshold crack nucleation is determined by extrapolating the tangential force amplitude related to a b_{pth} = 10 µm projected crack length. This strategy was systematically applied for all the studied conditions. The corresponding Q^*_{CN} values are compiled in table 2. The expertise shows that the incipient crack nucleation is systematically observed at the trailing contact borders. Note that under established partial slip conditions, the surface wear is negligible and the contact geometry assumed unchanged during the fretting tests.

4. Contact stress analysis

4.1. Fretting Fatigue Stress field computation

The contact stress analysis of studied plain fretting and fretting fatigue experiments is performed by applying an analytical formulation which consists to combine the Mindlin's analytical description of partial slip contact (Fig. 4a) [9] with an adequate application of the McEven formalism's [9].

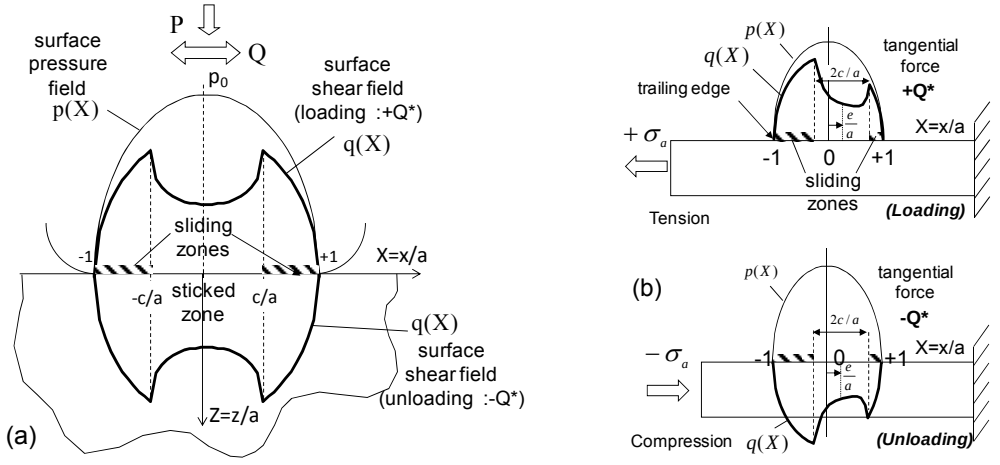

Figure 4. Pressure and Shear surface profiles under partial slip conditions a) plain fretting – b) fretting fatigue

The McEven formalism allows us to establish the stress state below the surface related to elliptical surface pressure or shear profiles. By summing the contribution of various elliptical shear distributions, the partial slip loading path can be determined. Note that the offset or eccentricity "e" of the stick zone, which induced by the fatigue strain deformation of the fatigue specimen, is considered by applying the Nowel's formalism [11] (Fig. 4b). This approach is justified if the

Hertzian hypotheses are satisfied which implies elastic stress conditions, smooth surfaces, plain strain hypothesis and thick enough specimen to satisfy the semi infinite contact configuration. The low surface roughness of specimens, the large lateral width of cylinder pads and the 10 mm specimen thicknesses support such hypothesis. Besides, a posteriori stress analysis shows that all the crack nucleation conditions correspond to elastic stress conditions ($\sigma_{VM}/\sigma_y < 1$). A major interest of this analytical stress description is the very fast computation of the cyclic stress path which allows an extensive non local multiaxial fatigue stress analysis.

4.2. Crossland's Multiaxial Fretting criterion

The stress loadings operating below the surface are multiaxial and therefore a multixial fatigue analysis is required. The Crossland's multiaxial fatigue approach [12], well adapted to describe the fatigue response of the studied alloy, is considered. The crack risk is expressed as a linear combination of the maximum amplitude of the second invariant of the stress deviator $\sqrt{J_{2,a}}$, and the maximum value of the hydrostatic pressure ($\sigma_{h,max}$) (Fig. 5a).

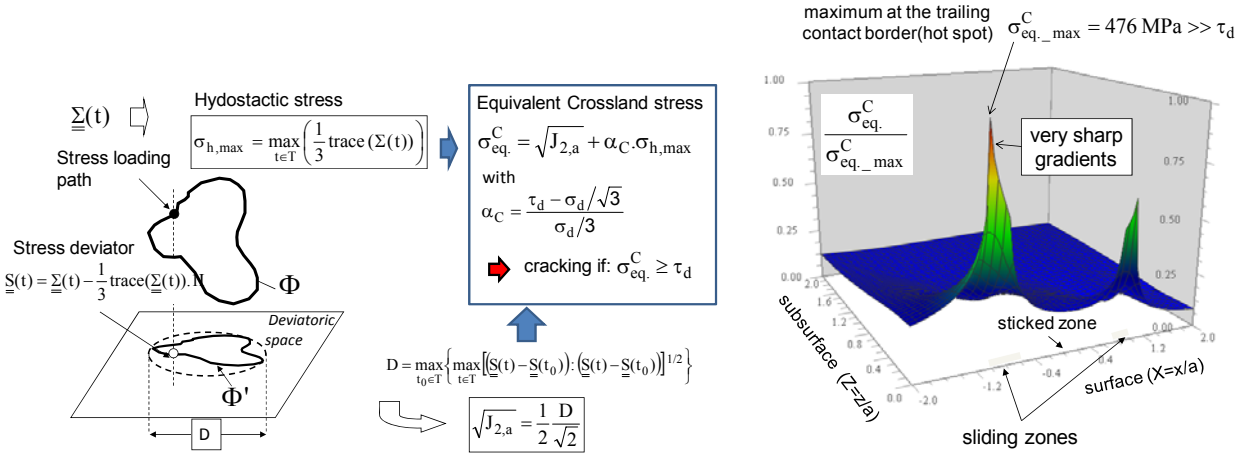

Figure 5. a) Illustration of the Crossland criterion – b) Crossland distribution of the FF2 condition (local stress analysis) (Table 2)

The crack nucleation condition is verify if the equivalent Crossland fatigue stress is becoming larger than the shear fatigue limit :

$$\sigma^{C}_{eq.} = \sqrt{J_{2,a}} + \alpha_C.\sigma_{h,max} \geq \tau_d \quad \text{with for the studied alloy} \quad \alpha_C = 0.28 \qquad (1)$$

Figure 5b shows the distribution of Crossland criterion computed for a representative Fretting Fatigue crack nucleation condition (i.e. FF2 test, Table 2) applying a local stress analysis. Confirming the experimental results, the maximum risk value is localized at the trailing contact border. The distribution shows very sharp gradients and a dissymmetry of the profile induced by stick zone offset generate by the fatigue mismatching strain deformation within the interface.

5. Comparison between experiments and fatigue modeling

5.1. Local « hot spot » fatigue analysis

The multaxial fatigue analysis is applied using a local stress description at the hot spot stress location (i.e. trailing contact border). The analysis is performed for each plain fretting and fretting fatigue crack nucleation conditions and reported in a $\sqrt{J_{2,a}}$ - $\sigma_{h,max}$ diagram (Fig. 6).

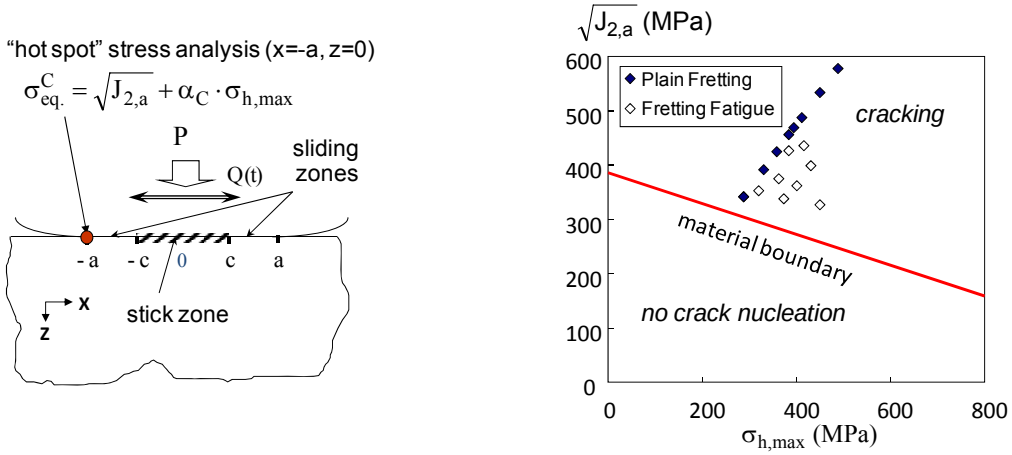

Figure 6. Local Crossland analysis at the "hot spot" trailing contact border.

As expected, the experimental data are highly dispersed and systematically above the material boundary. This local Crossland fatigue approach does not integrate the severe stress gradients operating next to the "hot spot" and therefore is not suitable to predict the fretting cracking risk. To quantify the stability of the prediction, the mean value and the square root variance of the equivalent Crossland stress obtained for the 16 test conditions are computed.

$$\overline{\sigma}_{eq.}^{C.} = \frac{1}{N}\sum_{i=1}^{N}\sigma_{eq.}^{C.}(i)\,,\quad \%E\overline{\sigma}_{eq.}^{C.} = \left(\frac{\overline{\sigma}_{eq.}^{C.} - \tau_d}{\tau_d}\right)x100\,,\quad V\sigma_{eq.}^{C.} = \sqrt{\frac{\sum_{i=1}^{N}\left(\sigma_{eq.}^{C.}(i) - \overline{\sigma}_{eq.}^{C.}\right)}{N-1}}\,,\quad \%V\overline{\sigma}_{eq.}^{C.} = \left(\frac{V\overline{\sigma}_{eq.}^{C.}}{\overline{\sigma}_{eq.}^{Cross.}}\right)x100 \qquad (2)$$

The $\%E\overline{\sigma}_{eq.}^{C}$ allows to estimate the global error of prediction versus the theoretical material prediction, whereas the $\%V\overline{\sigma}_{eq.}^{C}$ variable provides a relative estimation of the dispersion. For the given local fatigue description, we found $\%E\overline{\sigma}_{eq.}^{C}$ = +36 % and $\%V\overline{\sigma}_{eq.}^{C}$ = 16% which correspond to a critical overestimation and a high dispersion.

5.2. Non local « critical » distance fatigue approach

The critical distance method which consists to define the stress state at a certain distance below the contact "hot spot" (Fig. 7a) is applied. Using the Taylors's theory [13] which approximates the critical distance as the half value of the long crack propagation transition b_0, we deduced :

$$\lambda_T = \frac{b_0}{2} \approx \frac{1}{2\pi}\left(\frac{\Delta K_{th}}{\sigma_d}\right)^2 \approx 5\mu m \tag{3}$$

This strategy previously applied par Araujo et al. in [4] is now considered for the given Crossland's fatigue analysis (Fig. 7).

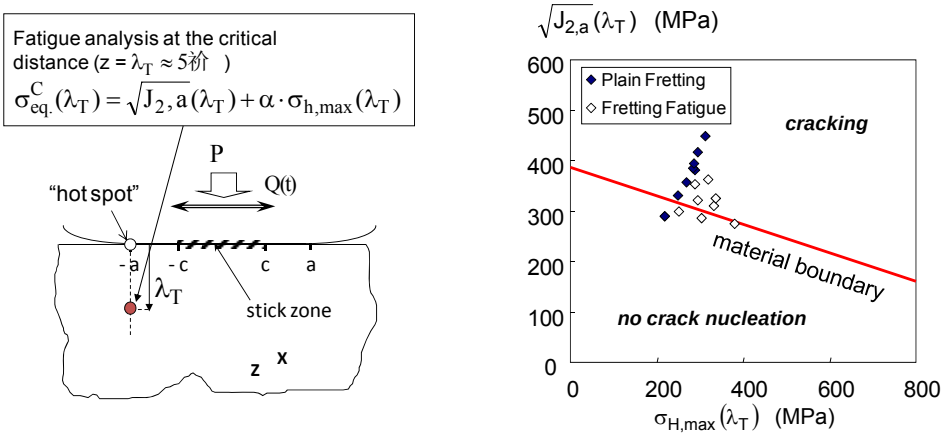

Figure 7: Critical distance approach assuming a constant length scale value ($\lambda_T = b_0/2 = 5\mu m$).

The experimental results are closer to the material boundary and the dispersion is reduced. The statistical analysis gives $\%E\overline{\sigma}^C_{eq.}(\lambda_T) = 11\%$ and $\%V\overline{\sigma}^C_{eq.}(\lambda_T) = 12\%$. The global predictions are less conservative but still dispersed. This suggests that the "critical distance" approach which consider a single "material" length scale parameter is not sufficient to fully capture the stress gradient for such very large stress gradient range.

5.3 Weigth function approach

An alternative non local approach which consists to consider the "hot spot" fatigue stress value weighted by a linear decreasing function (w) of the hydrostatic stress gradient surrounding the hot spot location is now considered [6, 7]:

$$\sigma^{C*}_{eq.} = \sigma^C_{eq.}.w\left(\left|\overline{\nabla}_\lambda(\sigma_{h\,max})\right|\right) \quad \text{where} \quad w = 1 - k.\left|\overline{\nabla}_\lambda(\sigma_{h\,max})\right| \tag{4}$$

With $\left|\overline{\nabla}_\lambda(\sigma_{h\,max})\right|$ the mean stress gradient of the hydrostatic stress over a cubic volume defined by the length scale λ. Hence for plain strain conditions it leads to

$$\left|\nabla(\sigma_{h,max}(x,z))\right| = \sqrt{\left(\frac{\partial\sigma_{h,max}}{\partial x}\right)^2 + \left(\frac{\partial\sigma_{h,max}}{\partial z}\right)^2} \tag{5}$$

which for the studied fretting conditions infers :

$$\left|\overline{\nabla}_\lambda(\sigma_{h\,max})\right| = \sqrt{\left(\frac{\sigma_{h,max}(-a,0) - \sigma_{h,max}(-a,\lambda)}{\lambda}\right)^2 + \left(\frac{\sigma_{h,max}(-a,0) - \sigma_{h,max}(-a+\lambda,0)}{\lambda}\right)^2} \tag{6}$$

The length scale λ is usually related to the grain size so that $\lambda = Ø/2 = 10\ \mu m$ which presently gives $k = 0.0142\ (MPa/\mu m)^{-1}$

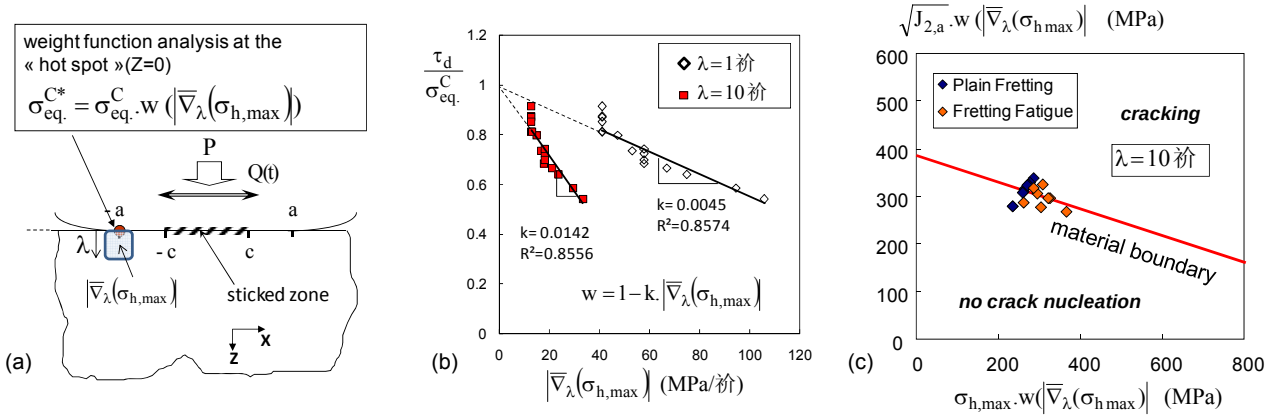

Figure 7: Weight function approach: a) illustration of the methodology- b) identification of the weight function – c) Application of the methodology (ℓ=Ø/2=10µm).

Using this weight function approach the predictions are highly improved. The statistical analysis gives $\%E\overline{\sigma}^{C*}_{eq.} = 1\%$ and $\%V\overline{\sigma}^{C*}_{eq.} = 6\%$. However, as shown in Fig. 7b, the "k" coefficient highly depends on the volume dimension over which the hydrostatic stress gradient is computed. The smaller the ℓ value, the higher the stress gradients, and smaller the k factor is. This suggests that the methodology must be calibrated keeping constant the ℓ dimension from the identification of the weight function to the structural fatigue analysis. By contrast, the R^2 coefficient is very stable which indirectly support the stability of this approach. Theses tendencies are confirmed by Figure 8, where using extensive computations, both "k and R^2" variables are plotted versus ℓ variable. The k variable can be expressed using a very simple power function at least for the studied cylinder/plane contact:

$$k = 5.10^{-3} \cdot \sqrt{\lambda} \tag{7}$$

Besides, the related R^2 coefficient remains unchanged around 0.85 whatever the ℓ value. Hence, it can be intuited that such approach could be transposed for any low spatial stress field resolution like observed in industrial FEM contact analysis. Fixing the ℓ variable equal for instance to the FEM contact mesh size and calibrating the related k weight function factor, very good prediction of the crack risk are expected.

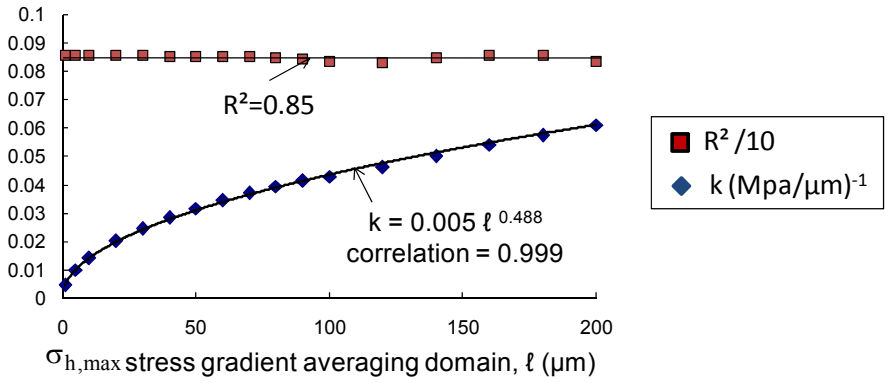

Figure 8: evolution of the k coefficient and related R^2 correlation factor as a function of the length scale ℓ.

5. Conclusion

A combined experimental and Crossland multiaxail fatigue approach is developed to rationalise the crack nucleation risk induced by plain fretting and fretting fatigue loadings. It shows that due to the very stress grading imposed by the contact stressing, a local “hot spot” fatigue stress analysis is not suitable. The application of the critical distance approach based on the Taylor’s formalism improves the prediction but still display high dispersion. Finally, the non local “weight function” approach provides very consistent and stable predictions. This analysis shows that the “k” factor defining weight function is highly dependent on the ℓ length scale variable over which the hydrostatic stress gradient is computed. We show a variation of the k factor versus the ℓ length variable. Finally, we confirm that the stability of this approach according that the related R^2 correlation factor remains high and constant (i.e. above 0.85) over the whole studied ℓ length (i.e. up to 200μm). This stability regarding the spatial stress resolution suggests that, this approach could efficiently be transposed in coarse industrial FEM contact meshing to achieve pertinent fretting cracking predictions.

References

[1] R.B. Waterhouse, Fretting Fatigue, Applied Science publishers, 1981.
[2] M.P. Szolwinski, T.N. Farris, Mechanics of fretting crack formation. Wear 1996;198:93-107.
[3] S. Fouvry, Ph. Kapsa, F. Sidoroff, L. Vincent, Identification of the characteristic length scale for fatigue cracking in fretting contacts. J. Phys. IV France 1998; 8: 159-166.
[4] J.A. Araújo, D. Nowell, The effect of rapidly varying contact stress fields on fretting fatigue. International Journal of Fatigue 2002; 24 (7): 763-775.
[5] S. Fouvry, K. Kubiak, Development of a fretting–fatigue mapping concept: The effect of material properties and surface treatments, Wear, 267(2009) 2186–2199
[6] IV. Papadopoulos. Int J Fatigue 2001;23:839–49.
[7] R. Amargier, S. Fouvry, L. Chambon, C. Schwob, C. Poupon, , Int. J of Fatigue,2010, 32 (12) : 1904-1912.
[8] L.J. Fellows, D. Nowell, DA. Hills, On the initiation of fretting fatigue cracks. Wear 1997;205:120–9.
[9] KL. Johnson, Contact Mechanics, Cambridge University Press,1985.
[10] H. Proudhon, S. Fouvry, J.-Y. Buffière, A fretting crack initiation prediction taking into account the surface roughness and the crack nucleation process volume. International Journal of Fatigue,2005; 27(5):569-579.
[11] D. Nowell, D.A. Hills,Mechanics of fretting fatigue tests, Int. Jnl. Mech. Sci., 1987, 29, 5: 355-365
[12] B. Crossland, Proceeding of the Inter. Conf. On Fatigue of Metals, Inst. of Mechanical Engineers, London, 1956, pp. 138-149.
[13] D. Taylor D. Analysis of fatigue failures in components using the theory of critical distances. Engng Fail Anal 2005;12:906–14.